A mathematical tool to generate complex whole body motor tasks and test hypotheses on underlying motor planning

Michele Tagliabue, Alessandra Pedrocchi, Thierry Pozzo, Giancarlo Ferrigno

Med Bio Eng Comput
DOI 10.1007/s11517-007-0252-4

ORIGINAL ARTICLE

A mathematical tool to generate complex whole body motor tasks and test hypotheses on underlying motor planning

Michele Tagliabue · Alessandra Pedrocchi · Thierry Pozzo · Giancarlo Ferrigno

Received: 23 March 2007 / Accepted: 31 July 2007

Abstract In spite of the complexity of human motor behavior, difficulties in mathematical modeling have restricted to rather simple movements attempts to identify the motor planning criterion used by the central nervous system. This paper presents a novel-simulation technique able to predict the "desired trajectory" corresponding to a wide range of kinematic and kinetic optimality criteria for tasks involving many degrees of freedom and the coordination between goal achievement and balance maintenance. Employment of proper time discretization, inverse dynamic methods and constrained optimization technique are combined. The application of this simulator to a planar whole body pointing movement shows its effectiveness in managing system nonlinearities and instability as well as in ensuring the anatomo-physiological feasibility of predicted motor plans. In addition, the simulator's capability to simultaneously optimize competing movement aspects represents an interesting opportunity for the motor control community, in which the coexistence of several controlled variables has been hypothesized.

Keywords Motor control · Optimization · Simulation · Posture · Pointing

1 Introduction

In the field of neuroscience, movement simulation is becoming increasingly important to test the reliability of neurophysiological theories proposed to explain efficient human motor behavior. The computational approach seems especially useful to study the neural mechanisms underlying the definition of the motor plan, often called the "desired trajectory", to accomplish a given task. Indeed, it is still matter of debate the nature of the processes occurring prior to movement execution that are aimed at solving the three indeterminacy problems involved in goal-oriented movement planning [24]: (1) determination of the endpoint trajectory in extrinsic coordinates; (2) selection of the best joint angle combinations able to produce the selected endpoint trajectory; (3) determination of muscle activations that will produce the planned kinematics.

Stereotyped features of human arm movements [7, 29, 41] suggest that the central nervous system (CNS) must use an optimality criterion to solve these indeterminacy problems, but its unequivocal identification is still an open point [1, 12, 17, 30, 42, 48, 51]. Although the proposed theories and the corresponding computational models have shed light on the neural processes underlying human motor planning, they show some important limitations. Indeed, since most of them focus on movement characterized by an equal number of degrees of freedoms (DoFs) in the joint and hand spaces, they entail a one-to-one correspondence between hand and

Supported by Italian Space Agency DCMC contract and by Italian Institute of Technology.

M. Tagliabue (✉) · A. Pedrocchi · G. Ferrigno
NITlab, Department of Bioengineering, Politecnico di Milano,
29 Via Garofalo, 20133 Milano, Italy
e-mail: michele.tagliabue@polimi.it

T. Pozzo
Faculté des Sciences du Sport, Université de Bourgogne,
Dijon, Campus Universitaire, BP 27877, 21078 Dijon, France

T. Pozzo
INSERM, U887, Dijon, France

T. Pozzo
Italian Institute of Technology, Genova, Italy

Journal : Large 11517 | Dispatch : 31-8-2007 | Pages : 12
Article No. : 252 | ☐ LE | ☐ TYPESET
MS Code : 252 | ☑ CP | ☑ DISK

joint angle trajectories. The resulting theories, therefore, cannot be easily generalized to more complex movements that require a solution to the second problem of indeterminacy. To this end, a breakthrough was achieved in the investigation and modeling of the final arm posture in movements where task achievement leaves one unconstrained DoF [1, 42].

The present work aims at broadening previous theories by considering tasks characterized by several DoFs, which better represent our everyday motor behavior. These movements require a simultaneous solution to the first- and second-order problems of indeterminacy. We address this goal by investigating and modeling transitive movements involving the whole body. By transitive motor act we mean the execution of a task with a defined visual goal, not inwardly perceived, and requiring the sensory–motor transformation, from visual to body space, which characterizes classical pointing movements. Moreover, by studying whole body transitive tasks performed from a standing position, a pivotal question in motor control, i.e., the coordination between hand trajectory formation and equilibrium maintenance [13, 36], could be explored. Previous studies, performed with intransitive task, like trunk bending [2] or arm raising [38], represent important steps in the understanding of the very general question of posture and movement coordination [27], therefore, they represent a natural starting point for the investigation of the coordination between balance and transitive task performance.

In the light of these considerations, it seems profitable to extend the modeling studies and related theories that have focused on both intransitive postural perturbation tasks and hand movements, to transitive whole body movements. However, this entails a remarkable increase in the complexity of the motor-control problem, due to the increase of the DoFs and to the intrinsic human posture instability. Therefore, previously developed simulation techniques would not be suitable. For this reason, the present paper aims at providing a tool allowing an easy application of classical planning criteria focused on movement kinetics, kinematics, balance or task accomplishment to whole body goal-oriented movements.

In the first part of the paper, the main structure of the simulator will be presented. Afterwards, as example of its possibilities, the simulator will be applied to a planar whole body pointing (WBP) task from standing, where the task accomplishment involves all body segments. This protocol was selected because it may be considered as an example of transitive complex movement, involving many DoFs and requiring a strong coordination between an explicit task fulfillment and equilibrium control. Furthermore, such a paradigm has led to several experimental investigations and provided a considerable amount of data [10, 19, 21, 36, 37, 43–46, 49]. In the subsequent part, an effective technique to combine several motor planning criteria is discussed. Indeed, since during WBP the CNS must solve several problems (i.e., spatial and postural), the possibility of simultaneously optimizing various aspects of the motor plan seems particularly desirable.

2 Methods

The simulator structure is reported in Fig. 1. The approach used is based on an iterative optimization algorithm that searches for the movement kinematics which minimize a cost function explicitly defined to describe a specific motor

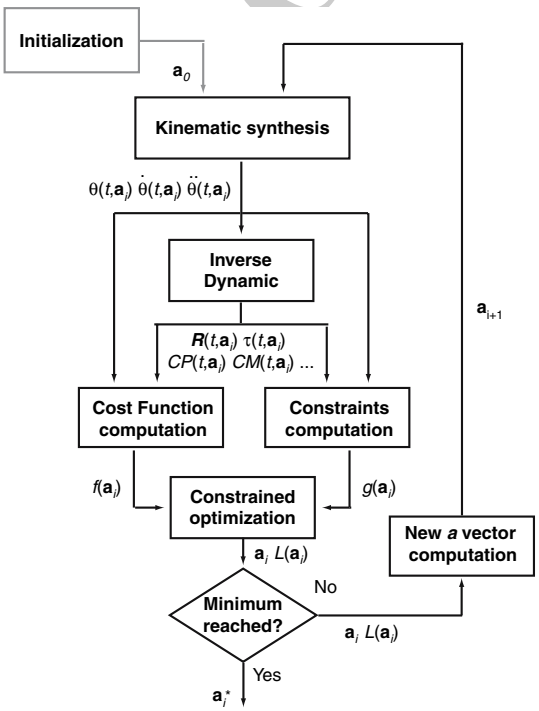

Fig. 1 Block diagram representing the simulator iterative structure. At the *i*th iteration of the optimization process, $\mathbf{a}_i$ is a matrix of coefficients used to synthesize body segments' angular position velocity and acceleration, $\theta, \dot{\theta}$ and $\ddot{\theta}$ (kinematic synthesis block). The obtained kinematics is fed to the "Inverse dynamic" block that computes joint reaction forces and torques, $\mathbf{R}$ and $\boldsymbol{\tau}$, as well as other parameters as the center of mass (CM) and the center of pressure (CP). Both kinematics and kinetics go through the "Cost function computation" and the "Constraints computation" blocks, which respectively evaluate the cost figure to be minimized, $f(\mathbf{a}_i)$, and the constraint fulfillment, $\mathbf{g}(\mathbf{a}_i)$. Then, the "Constrained optimization" block combines these two functions in the Lagrangian function, $L(\mathbf{a}_i)$, to evaluate whether or not the algorithm reached the minimum of the cost function. If not, a new vector $\mathbf{a}_{i+1}$ corresponding to a lower value of the Lagrangian function is computed and a new iteration starts, otherwise the actual set of coefficients, $\mathbf{a}^*_i$, corresponding to the optimal movement execution, is returned. The initialization is carried out by the "initialization" block that produces a starting matrix of coefficients, $\mathbf{a}_0$

Journal : Large 11517 Dispatch : 31-8-2007 Pages : 12
Article No. : 252 LE TYPESET
MS Code : 252 CP DISK

strategy. A more detailed functional description of the blocks of the diagrams in Fig. 1 is reported in the following paragraphs.

2.1 Synthesis of the movement kinematics

To reduce the dimensionality of the optimization problem, the trajectories of the angular DoFs of the system, $\theta(t)$, (see Fig. 2) are computed as weighted sums of B-spline functions [52], as reported in (1). In this way, the dimension of the angular trajectory space basis corresponds to the number of coefficients $a_{j,k}$.

$$\theta_k(t, \mathbf{a}) = \sum_{j=1}^{N} B_{jW}(t) \cdot a_{j,k} \qquad k = 1, \ldots, s \tag{1}$$

where $B_{jW} = B(.| t_j, \ldots, t_{j+W})$ is the jth B-spline of order W, N is the number of coefficients (14 in the implementation) in each column of **a** matrix (with elements $a_{j,k}$) and s is the number of model segments and the size of rows of the matrix **a** (5, as shown in Fig. 2). Therefore, the total number of coefficients $a_{j,k}$ is $N{\cdot}s = 70$ and $\Re^{N \cdot s}$ is the optimization solution space basis. The selected spline order, W, is 8. Such values for N and W ensure a sufficient spline flexibility, even if the body segments orientation, velocity and acceleration at the first frame are constrained. Moreover, such a high order does not automatically force to zero jerk angle profiles as do third order piecewise polynomials.

The kinematic synthesis block also computes segment angular velocity and acceleration $(\dot{\theta}, \ddot{\theta})$.

2.2 Initialization

Movement kinematics of six voluntary subjects performing WBP tasks were recorded by a motion capture system (for experimental protocol details, see [37]). The symmetry of the task allows it to be modeled in the sagittal plane alone, without loss of significant information. Therefore, only joint angle projections onto the sagittal plane were considered.

Angular trajectories of the segments are computed by fitting B-splines to the average of the experimentally measured behavior. Then, the initial **a** matrix is defined by adding random noise to the coefficients of the interpolating B-splines. The noise maximum amplitude is set to 5% of

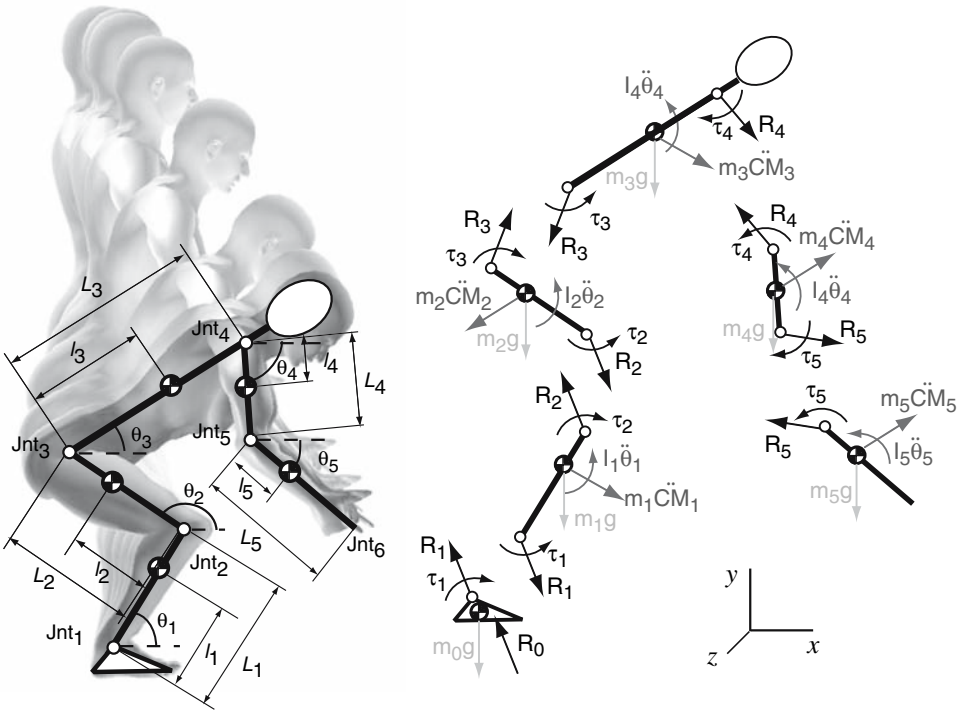

Fig. 2 On the left, a schematic representation of the whole body pointing (WBP) protocol is shown. For the final position (*darker cartoon*) the biomechanical model used to describe the human body is superimposed. Jnt_{1-6} are ankle, knee, hip, shoulder, elbow and index finger apex position. θ_{1-5} are the shank, leg, trunk, arm and forearm angular position. L_{1-5} are the body segments' length. l_{1-5} are the distance between the segments' CM, represented by *crossed circles*, and the distal joint. To improve figure legibility, all trimming parameters Δl and Δtr are assumed to be zero. On the right, a representation of the inverse dynamic solution is reported. m_k and I_k are the mass and inertial moment of the kth segment. $\ddot{\theta}_k$ and $\ddot{\text{CM}}_k$ are the segment angular and linear acceleration. $\mathbf{R}_k$ and $\boldsymbol{\tau}_k$ are the reaction force and torque at the kth joint

Journal : Large 11517 Dispatch : 31-8-2007 Pages : 12
Article No. : 252 LE TYPESET
MS Code : 252 CP DISK

the **a** elements mean value. Greater noise tends to prevent the convergence of the algorithm because it locates the starting point of the minimum search far from the subspace corresponding to the physiological solutions.

2.3 Inverse dynamic method

The synthetized kinematic time course is applied to the biomechanical model of the human body reported in Fig. 2. The position ($x(t)$, $y(t)$, $z(t)$) of each joint (Jnt) is computed as follows:

$$\mathbf{Jnt}_k(t,\mathbf{a}) = \mathbf{Jnt}_{k-1}(t,\mathbf{a}) + L_{k-1}\cdot\mathbf{v}_{k-1}(t,\mathbf{a}) \quad k = 2,\ldots,N \quad \text{with} \quad \mathbf{Jnt}_1(t,\mathbf{a}) = (0,0,0) \quad \forall t \tag{2}$$

where $\mathbf{v}_k(t,\mathbf{a})$ is a unit vector, defined as

$$\mathbf{v}_k(t,\mathbf{a}) = [\cos(\theta_k(t,\mathbf{a})) \quad \sin(\theta_k(t,\mathbf{a})) \quad 0]$$

describing the kth body segment orientation and L_k is its length. The constant zero value of the third component of the unit vector $\mathbf{v}_k$ is due to the choice of applying the simulator to a planar movement. Also kth body segments center of mass (CM) position is evaluated using equation 3:

$$\mathbf{CM}_k(t,\mathbf{a}) = \mathbf{Jnt}_k(t,\mathbf{a}) + (l_k + \Delta l_k)\cdot\mathbf{v}_k(t,\mathbf{a}) + \Delta\mathrm{tr}_k\cdot\mathbf{n}_k(t,\mathbf{a}) \tag{3}$$

where l_k is the nominal distance of the segment CM from the distal joint as defined by anthropometrical tables, $\mathbf{n}_k$ is a unit vector normal to $\mathbf{v}_k$ defined as

$$\mathbf{n}_k(t,\mathbf{a}) = [-\sin(\theta_k(t,\mathbf{a})) \quad \cos(\theta_k(t,\mathbf{a})) \quad 0]$$

and Δl_k and $\Delta\mathrm{tr}_k$ are CM position corrections along longitudinal and transversal directions respectively, which are defined during the biomechanical model validation. These trimming parameters minimize the differences between the ground reaction forces and the CP position, estimated by using the inverse dynamics method (IDM) on motion capture system data and the force platform data, recorded during subjects' WBP task executions [23]. Acceleration of CMs is evaluated using equation 4:

$$\ddot{\mathbf{CM}}_k(t,\mathbf{a}) = \sum_{i=1}^{k-1} L_i\left(\ddot{\theta}_i(t,\mathbf{a})\cdot\mathbf{n}'_i(t,\mathbf{a}) - \dot{\theta}_i^2(t,\mathbf{a})\cdot\mathbf{v}'_i(t,\mathbf{a})\right) + l'_k\left(\ddot{\theta}_k(t,\mathbf{a})\cdot\mathbf{n}'_k(t,\mathbf{a}) - \dot{\theta}_k^2(t,\mathbf{a})\cdot\mathbf{v}'_k(t,\mathbf{a})\right) \tag{4}$$

where $\mathbf{v}'_k$, $\mathbf{n}'_k$, l'_k are modifications of the corresponding parameters due to the corrections of the CM position, Δl_k and $\Delta\mathrm{tr}_k$, analytically defined as:

$$\mathbf{v}'_k(t,\mathbf{a}) = [cos(\theta'_k(t,\mathbf{a})) \quad sin(\theta'_k(t,\mathbf{a})) \quad 0]$$
$$\mathbf{n}'_k(t,\mathbf{a}) = [-sin(\theta'_k(t,\mathbf{a})) \quad cos(\theta'_k(t,\mathbf{a})) \quad 0]$$
$$l'_k = \sqrt{(l_k + \Delta l_k)^2 + (\Delta\mathrm{tr}_k)^2}$$

with

$$\theta'_k(t,\mathbf{a}) = \theta_k(t,\mathbf{a}) + \arctan\left(\frac{\Delta\mathrm{tr}_k}{l_k + \Delta l_k}\right)$$

Movement kinetics are estimated using the IDM. The IDM consists of the sequential solution of the equilibrium equations (5) and (6), from the endpoint to the ankle joint (k = 5,…, 1):

$$\mathbf{R}_k(t,\mathbf{a}) = m_k\cdot\ddot{\mathbf{CM}}_k(t,\mathbf{a}) + m_k\cdot\mathbf{g} + \mathbf{R}_{k+1}(t,\mathbf{a}) \tag{5}$$

$$\boldsymbol{\tau}_k(t,\mathbf{a}) = I_k\cdot\ddot{\theta}_k(t,\mathbf{a}) + \boldsymbol{\tau}_{k+1}(t,\mathbf{a}) + [\mathbf{Jnt}_{k+1}(t,\mathbf{a}) - \mathrm{CM}_k(t,\mathbf{a})]\wedge\mathbf{R}_{k+1}(t,\mathbf{a}) - [\mathbf{Jnt}_k(t,\mathbf{a}) - \mathrm{CM}_k(t,\mathbf{a})]\wedge\mathbf{R}_k(t,\mathbf{a}) \tag{6}$$

with

$$\mathbf{R}_6(t,\mathbf{a}) = \boldsymbol{\tau}_6(t,\mathbf{a}) = (0,\,0,\,0) \quad \forall t$$

where $\mathbf{R}_k$ and $\boldsymbol{\tau}_k$ are the joint reaction force and torque at the kth joint, m_k and I_k are the kth body segment mass and inertial moment (effects of the trimming parameters, Δl_k and $\Delta\mathrm{tr}_k$, on I_k were assumed to be negligible) and **g** is the gravity acceleration vector. Moreover, solving (5) and (6) also for the feet (k = 0), ground reaction forces and the antero-posterior position of the CP are evaluated. The CP position computation is possible because torque exchanged between feet and floor in medio-lateral direction is zero and the vertical coordinate of the CP always corresponds to the floor level. Moreover, to represent the experimental protocol characteristics the feet are assumed to be still ($\ddot{\mathrm{CM}}_0 = 0$ and $\ddot{\theta}_0 = 0$).

Biomechanical model parameters, L, l', m and I are defined as the average values obtained for the six voluntary subjects using anthropometrical tables [53] and the trimming procedure [23].

2.4 Computation of the constraints

As shown in Fig. 1, both kinematics and kinetics of the current solution go through the constraint block (CB). The solution has to fulfill two constraints: task constraints and anatomo-physiological constraints.

2.4.1 Task constraints

Task constraints concern the kinematic variables and are represented by (7)–(12). Equation (7), where $\bar{\theta}_k$ are the

Journal : Large 11517 | Dispatch : 31-8-2007 | Pages : 12
Article No. : 252 | LE | TYPESET
MS Code : 252 | CP | DISK

initial segment angular positions, defines the starting posture, while (8) and 9 impose its steadiness.

$$\theta_k(0,\mathbf{a}) = \bar{\theta}_k \quad k = 1,\ldots,5 \tag{7}$$

$$\dot{\theta}_k(0,\mathbf{a}) = 0 \quad k = 1,\ldots,5 \tag{8}$$

$$\ddot{\theta}_k(0,\mathbf{a}) = 0 \quad k = 1,\ldots,5 \tag{9}$$

Task accomplishment constraint is defined by imposing the endpoint position at the final instant, t_f, as shown in equation 10. Moreover, to guarantee a final steady body configuration, the angular segments velocity and acceleration must be zero (equations 11 and 12).

$$\mathbf{Jnt}_6(t_f,\mathbf{a}) = \bar{\mathbf{Jnt}}_6 \tag{10}$$

$$\dot{\theta}_k(t_f,\mathbf{a}) = 0 \quad k = 1,\ldots,5 \tag{11}$$

$$\ddot{\theta}_k(t_f,\mathbf{a}) = 0 \quad k = 1,\ldots,5 \tag{12}$$

2.4.2 *Anatomo-physiological constraints*

Anatomo-physiological constraints are aimed at representing the motor system characteristics. First, the task execution must be compatible with the range of motion of human joints. Second, joint torques, $\boldsymbol{\tau}_k(t,\mathbf{a})$, evaluated by using IDM, must be smaller than the maximum torque exertable by the muscles acting on the kth joint, $T_k(\theta,\dot{\theta})$. For each muscle group, a surface representing the maximal exertable torque, depending on joint angle position and velocity, was evaluated. In order to accurately represent the actual physiological muscle characteristics, in vivo measurements reported in the literature were used [18, 26, 31, 55]. Published data were also integrated by specific experimental acquisition using a Cybex isokinetic device. Obtained data were used to define the parameters of a simplified version of the Hill equation [35], representing the relationship between the maximal force and the muscle lengthening speed. An example of resulting surfaces is shown in Fig. 3. These constraints are important because the optimum search must take into account that joints develop different torques and that even the same joint cannot produce the same maximal torque in all conditions.

A further imposed constraint reflects the muscles' incapability of producing excessively abrupt joint torque changes, due to excitation and activation dynamics. In the model, torques evaluated applying the IDM must not require muscular neural inputs to be less than zero or greater than one. This would indicate that the required muscle activation level is prevented due to muscular

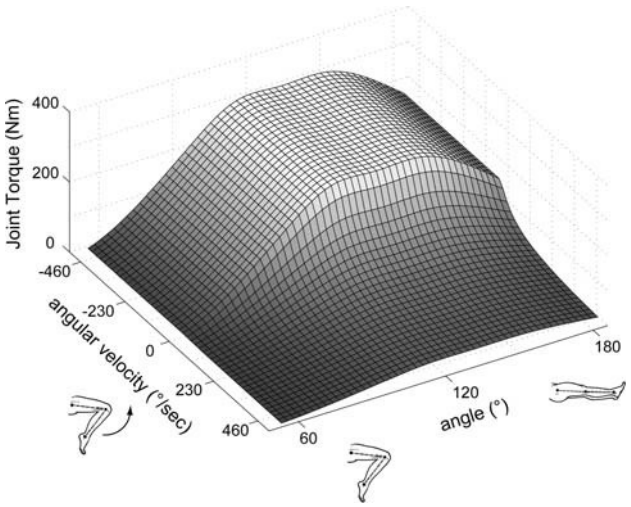

Fig. 3 Surface representing the maximal extensor torque as a function of angular velocity and angular position for the knee joint

dynamics [16]. Therefore, the constraint block must check that the muscle neural inputs, U, remain between 0 and 1. To estimate U, firstly, active joint torque components, $A\boldsymbol{\tau}_k$, are evaluated as differences between the net joint torques, obtained by the IDM, and the passive components calculated by using mathematical models representing joint stiffness, $\boldsymbol{\tau}_{k,\mathrm{stiff}}$, and viscosity, $\boldsymbol{\tau}_{k,\mathrm{visc}}$ [30, 39, 40, 54];

$$A\boldsymbol{\tau}_k(t) = \boldsymbol{\tau}_k(t,\mathbf{a}) - \boldsymbol{\tau}_{k,\mathrm{stiff}}(\boldsymbol{\theta}(t,\mathbf{a})) - \boldsymbol{\tau}_{k,\mathrm{visc}}(\dot{\boldsymbol{\theta}}(t,\mathbf{a})) \tag{13}$$

For each joint, active torque components are separated in flexor and extensor muscles contributions ($A\boldsymbol{\tau}_{k,1}$ and $A\boldsymbol{\tau}_{k,2}$, respectively) taking into account the minimal cocontractions necessary to physiological transitions from a muscle group to its antagonist. In particular, the same amount of active torque is added to agonist and antagonist muscles to produce a gradual transition between active and inactive muscle states (and vice versa). Transitions are represented by a fifth order polynomial that guarantees the continuity up to the second derivative. Afterward, an approximation of the contraction level, A, is computed as the ratio between the active torque components and their corresponding maximal value.

$$A_{k,i}(t,\mathbf{a}) = \frac{A\boldsymbol{\tau}_{k,i}(t,\mathbf{a})}{T_{k,i}(\theta(t,\mathbf{a}),\dot{\theta}(t,\mathbf{a}))} \quad k = 1,\ldots,5 \quad i = 1,2 \tag{14}$$

Finally, a rough estimation of the muscle motor commands is evaluated by inverting two first order differential equations representing muscle activation and excitation dynamics [16] (equations 15 and 16, respectively).

Journal : Large 11517 Dispatch : 31-8-2007 Pages : 12
Article No. : 252 LE TYPESET
MS Code : 252 CP DISK

$$E_{k,i,f-1} = \frac{A_{k,i,f} - A_{k,i,f-1} \cdot e^{-\frac{\Delta t}{T_a}}}{1 - e^{-\frac{\Delta t}{T_a}}} \quad (15)$$

$$U_{k,i,f-1} = \frac{E_{k,i,f} - E_{k,i,f-1} \cdot e^{-\frac{\Delta t}{T_e}}}{1 - e^{-\frac{\Delta t}{T_e}}} \quad (16)$$

$E_{k,i,f}$, $U_{k,i,f}$ are the excitation and the corresponding neural input of muscle groups acting on the kth joint at frame f. $\Delta t = 0.1$ ms is the sampling period used to allow the effective numerical solution of the differential equations describing muscular dynamic. T_a and T_e are muscle activation and excitation time constants: $T_a = 10$ ms and $T_a = 50$ ms during muscle activation and deactivation respectively, and T_e value is = 40 ms [16]. The employed muscle model does not certainly intend to accurately describe the single muscle dynamics, but it aims, by imposing the neural input to range between 0 and 1, only at roughly representing the impossibility of muscles groups to produce abrupt changes in their contraction level.

The last constraint represents the need to keep the balance ensuring that the CP always lies within the supporting base.

If one of the constraints is not fulfilled, CB output $\mathbf{g}(\mathbf{a})$ ($\mathbf{g}(\mathbf{a}):\Re^{N\cdot s} \rightarrow \Re^{m}$, where m is the constraints' number) has positive elements that penalize the current solution, as described in Sect. 2.6.

2.5 Motor planning criteria

Kinematics and kinetics, corresponding to the current combination of elements of matrix $\mathbf{a}$, are used in the cost function block (CFB) to evaluate the cost figure, $f(\mathbf{a})$, representing the motor planning criteria under evaluation. In the literature, several mathematical formulations, such as the minimum endpoint jerk model [12], the minimum torque change model [51] and the minimum commanded torque change models [30], were proposed.

As an example, two of the expressions, which will be used later on, are reported in (17) and (18). The first one, where Jnt_6 are the endpoint coordinates, represents the minimum Jerk model; while the second equation, where x_{CM} is the antero-posterior position of the whole body center of mass and $\bar{x}_{CM}$ is its mean value, is an implementation of the CM stabilization criterion, σ^2_{CM} [28].

$$\mathrm{Jerk} = \frac{1}{2}\int_0^{t_f}\left[\left(\frac{d^3\mathrm{Jnt}_{6,x}}{dt^3}\right)^2 + \left(\frac{d^3\mathrm{Jnt}_{6,y}}{dt^3}\right)^2\right] \cdot dt \quad (17)$$

$$\sigma^2_{CM} = \frac{1}{t_f}\int_0^{t_f}(x_{CM}(t) - \bar{x}_{CM})^2\, dt \quad (18)$$

2.6 Optimization algorithm

The simulator solves the following minimization problem:

$$\underset{\mathbf{a}\in\Re^{N\cdot s}}{\text{minimize}} \quad f(\mathbf{a}) \quad (19)$$

$$\text{subject to} \quad g_i(\mathbf{a}) = 0 \quad i = 1, \ldots, m_e \quad (20)$$

$$g_i(\mathbf{a}) \leq 0, \quad i = m_e + 1, \ldots, m \quad (21)$$

where m is the total number of imposed constraints and m_e is the number of these constraints represented by equality.

Therefore, at each iteration, the optimization algorithm block modifies the $\mathbf{a}$ matrix to reduce the cost function value fulfilling the imposed constraints.

The constrained optimization problem reported in equations (19)–(21) can be solved as an unconstrained one using the Lagrange function defined in (22).

$$L(\mathbf{a}, \boldsymbol{\lambda}) = f(\mathbf{a}) + \sum_{i=1}^{m} \lambda_i \cdot g_i(\mathbf{a}) \quad (22)$$

where $\boldsymbol{\lambda}$ is the vector of Lagrange multipliers. For a more detailed description of the optimization algorithm see [9].

To minimize the local minima problem, the simulator carries out several minimum searches starting from different points of the solution hyperspace and selecting the minimum among all the final solutions.

2.7 Combination of cost figures

To efficiently build a multiple cost function it is necessary to use a proper procedure to normalize the single cost functions that have to be combined. The normalization procedure must solve two problems: dimensional inconsistencies and differences in magnitude. The formula used is reported in (23),

$$\mathrm{NCF}_i = \frac{(\mathrm{CF}_i - \mathrm{CF}_{i,\min})}{(\mathrm{CF}_{i,\mathrm{real}} - \mathrm{CF}_{i,\min})} \quad (23)$$

where CF_i is the cost function to be normalized. $\mathrm{CF}_{i,\min}$ is the minimum value obtained by minimizing it individually. $\mathrm{CF}_{i,\mathrm{real}}$ is the value of the CF corresponding to the average experimental behaviour. By using this equation, all the normalized CFs (NCFs) are non-dimensional, have their minimum at zero and their values tend to vary in comparable ranges. NCFs can then be combined together to obtain the multiple cost function (MCF) of equation 24.

In order to allow weighting differently the single NCF_i a set of weights ($W_{\mathrm{NCF}i}$) can be defined according to the constraints shown in (25), (26). Therefore, $W_{\mathrm{NCF}i}$

Journal : Large 11517 | Dispatch : 31-8-2007 | Pages : 12
Article No. : 252 | LE | TYPESET
MS Code : 252 | CP | DISK

Table 1 The values and results of biomechanical model and Inverse dynamic method validation

	Segment										RMSE					
	1		2		3		4		5		CP		F_x		F_y	
	Δl	Δtr	Δl	Δtr	Δl	Δtr	Δl	Δtr	Δl	Δtr	B	A	B	A	B	A
S1	21	–53	11	–48	–33	–32	–17	10	–36	10	28	9	12	11	3	3
S2	21	24	–24	31	–35	–26	17	–10	40	–10	26	12	15	13	5	5
S3	19	–27	22	0	–5	–2	–16	–10	–36	–10	16	6	10	8	3	3
S4	18	–48	21	–20	–27	12	15	10	–1	10	18	9	12	11	5	5
S5	18	18	26	–26	–18	51	–5	–5	–17	–13	13	5	12	8	9	2
S6	–18	18	27	27	6	60	–5	–5	–59	–52	27	9	14	8	7	5
Med	18	–4	22	–10	–23	5	–5	–5	–27	–10	22	9	13	10	5	4
Quart	1	31	6	22	12	31	12	8	16	8	5	1	1	1	1	1

In the first part of the table the values of the biomechanical model trimming parameters (Δl and Δtr) are reported, in mm, for each body segment (1: shank, 2: leg, 3: Trunk & Head, 4: arm, 5: forearm&hand) and for each subject (S1–6). The second part of the table represents the results of the biomechanical model and Inverse dynamic method validation. For each subject, the table reports the percentage root mean squared error (RMSE%) between the antero-posterior centre of pressure positions (CP), the antero-posterior and vertical ground reaction forces (F_x, F_y) evaluated using the inverse dynamic method and the corresponding data recorded by using a force platform during the motor task execution. For each of these comparison the results obtained before, B, and after, A, the use of the above cited trimming parameters are reported. In the last two rows, median (Med) and the quartile (Quart) evaluated on six subjects are reported for all results

396 represents the fraction of the MCF due to the NCF_i.

$$MCF = 100 \cdot \sum_{i=1}^{V} W_{NCFi} \cdot NCF_i \quad (24)$$

398

$$\text{subject to} \quad \sum_{i=1}^{V} W_{NCFi} = 1 \quad (25)$$

400

$$W_{NCFi} \geq 0 \quad (26)$$

402 A multiplying global factor (i.e., 100) is also used to have
403 an MCF order of magnitude able to maximize the optimi-
404 zation algorithm efficiency. The number of cost figures (V)
405 that can be combined is theoretically unlimited.

406 ## 3 Results

407 ### 3.1 Biomechanical model and inverse dynamic method
408 validation

409 Table 1 shows the set of trimming parameters, Δl_k and
410 Δtr_k, and the corresponding validation improvements for
411 each subject. Table 1 also reports the median values of the
412 trimming parameters, which are applied to the biome-
413 chanical model used by the simulator.

414 A representative example of the model validation is
415 shown in Fig. 4. A remarkable match between the IDM
416 results and force platform data can be observed for the
417 antero-posterior CP position and the vertical component of

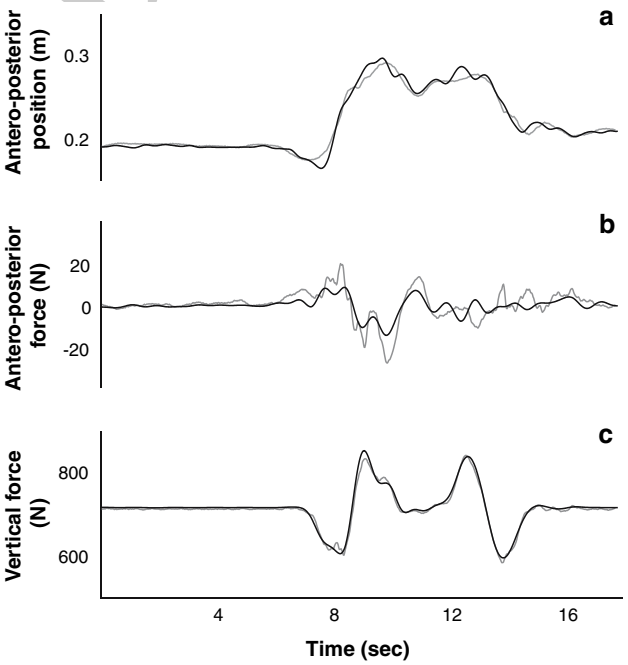

Fig. 4 Example of the validation of the biomechanical model and inverse dynamic methods. The data acquired by the force platform on which the subjects stood (*gray lines*) are compared with the corresponding data calculated by means of the inverse dynamics (*black lines*). In **a**, the antero-posterior position of the center of pressure is reported. Panels **b** and **c** show the antero-posterior and the vertical components of the ground reaction forces, respectively. The comparison has been made over the whole acquisition, including the period when the subject came back to the initial position

Journal : Large 11517 Dispatch : 31-8-2007 Pages : 12
Article No. : 252 LE TYPESET
MS Code : 252 CP DISK

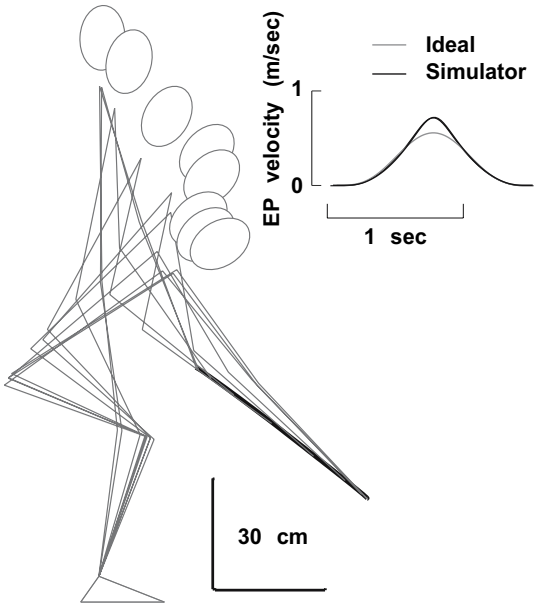

Fig. 5 Minimum endpoint jerk model prediction for WBP. The stick diagram represents the movement execution corresponding the minimization of the third derivative of the endpoint coordinated in a Cartesian reference frame. The resulting endpoint trajectory and velocity profiles (*thick lines*) are compared with the ideal minimum endpoint jerk trajectory (*gray lines*)

the ground reaction forces. Considering the necessary simplifications introduced by the biomechanical model, such results can be considered fully satisfactory.

3.2 Whole body movement simulation

Because of the instability and the relevant nonlinearities of the system and the high number of controlled DoFs, the simulator's effectiveness in minimizing a given cost figure could, in theory, not be optimal for WBP. In order to verify whether and how the increased problem complexity would significantly affect performance, the simulator was tested on three different motor planning models: minimum jerk, CM stabilization and CP stabilization. Their ideal solution is well-known, therefore, the discrepancies between the obtained results and the corresponding ideal solution can be used to evaluate the simulator's performance.

For instance, for simple and unconstrained hand movements starting from the (x_0, y_0) position, with null velocity and acceleration, and arriving after t_f seconds at the (x_{t_f}, y_{t_f}) position, the minimum jerk model, Jerk, represented by (17), produces an ideal finger trajectory described by (27) and (28) [12].

$$x(t) = x_0 + (x_0 - x_{t_f}) \cdot (15\tau^4 - 6\tau^5 - 10\tau^3) \quad (27)$$

$$y(t) = y_0 + (y_0 - y_{t_f}) \cdot (15\tau^4 - 6\tau^5 - 10\tau^3) \quad (28)$$

Figure 5 shows a qualitative comparison between this ideal hand path and simulation results for the Jerk minimization. No differences can be noticed for the endpoint trajectory morphology and only slight differences can be observed between velocity profiles. In fact, evaluation of the differences between the time courses of the endpoint coordinates obtained by simulation and by using (27) and (28) gives a root mean squared error below 1 cm, corresponding to about 1% of the whole distance covered by the finger.

For CM variance minimization (equation 18), the full antero-posterior stabilization $\sigma^2_{CM} = 0$, was considered as ideal solution [27, 28]. Simulation results for σ^2_{CM} are reported in Fig. 6. Panel B clearly shows that the simulator is perfectly able to stabilize the whole body CM (σ_{CM} = 0.06 mm) respecting all task and anatomo-physiological constraints.

As we did for the CM (equation 18), the cost function representing the CP stabilization model consists of its antero-posterior variance, σ^2_{CP}; therefore its full stabilization, $\sigma^2_{CP} = 0$, was considered as the ideal model prediction. Despite the fact that the σ^2_{CP} model introduces relevant nonlinear kinetics components with respect to σ^2_{CM}, even

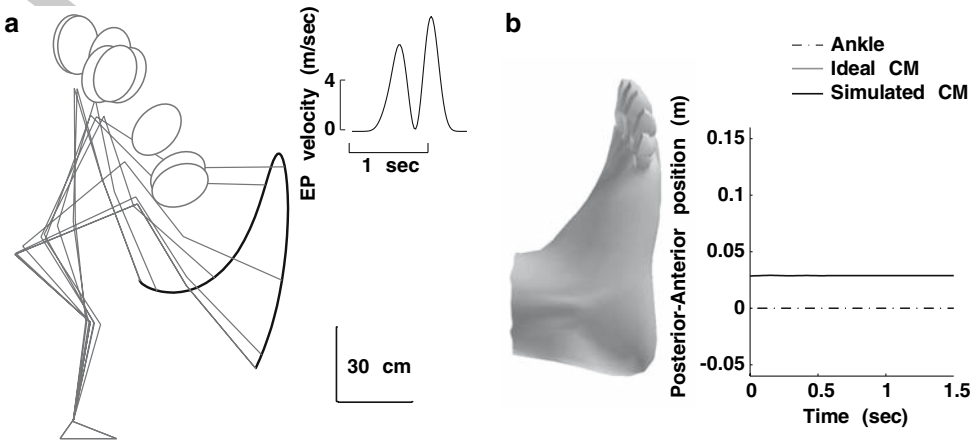

Fig. 6 Minimum center of mass displacement model prediction for WBP. In **a** the stick diagram, representing the movement execution corresponding to this motor planning model, is reported together with the end point trajectory (*thick line*) and the endpoint velocity profile (*upper-right corner*). Panel **b** shows the anterior-posterior position of the center of mass (CM) during movement execution

Journal : Large 11517 Dispatch : 31-8-2007 Pages : 12
Article No. : 252 LE TYPESET
MS Code : 252 CP DISK

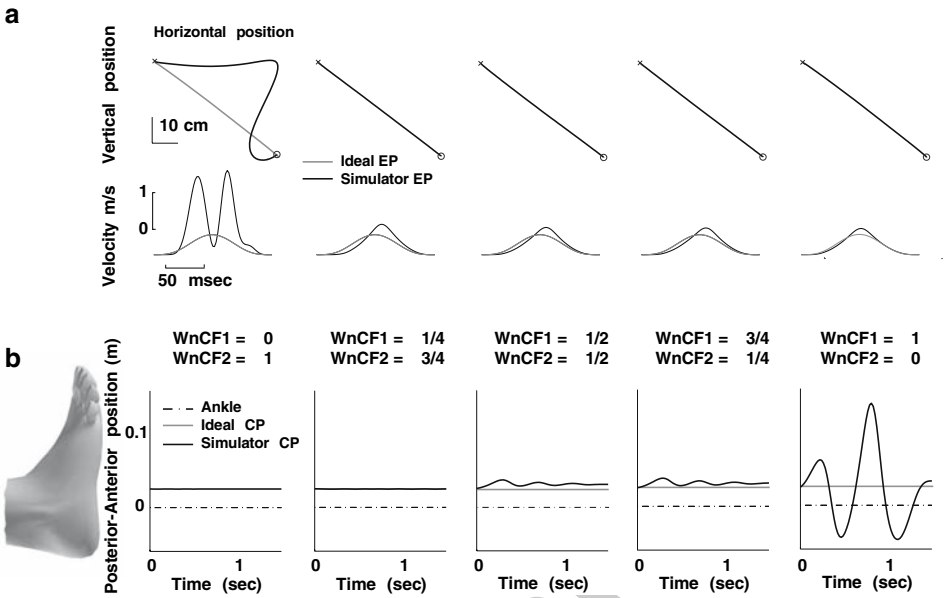

Fig. 7 Combination of two cost functions. Predictions corresponding to five combinations of the minimum jerk (Jerk) and the minimum center of pressure displacement (σ^2_{CP}) models are reported. In **a** the Jerk theoretical endpoint trajectory and velocity profiles (*gray lines*) are compared with the simulator predictions (*black lines*); **b** represents the comparison between the fully stabilized CP antero-posterior position (*gray lines*) and the simulation results (*black lines*). WnCF1 and WnCF2 are the weights given to the Jerk and σ^2_{CP} models, respectively

more accurate results (σ_{CP} = 0.03 mm) were obtained. Besides showing the simulator reliability in searching optimal strategies, WBP execution predicted by this model seems realistic, because resulting large and complicate upper limbs movements, shown in the first column of Fig. 7, resemble equilibrist walking on the tightrope, i.e., keeping the CP stable. In both simulator and funambulist behaviours inertial effects of wide arm movements aim at compensating unbalancing due to the rest of the body.

Besides being effective, the simulator proves reliable. Having performed ten simulations for each of the three tested CFs, the average deviation from the best solution is below 5%.

3.3 Combination of motor planning criteria

In order to test the efficiency of the simulator with MCFs, different combinations of Jerk and σ^2_{CP} models were implemented. These two models were selected because they focus on different aspects of the movements (focal and postural) and together they involve both movement kinematics and kinetics, therefore, their combination represents a relevant test of the simulator's capabilities.

As expected, results, reported in Table 2 and in Fig. 7, show that the lower the weight of the NCFs the bigger the discrepancies between the MCF model predictions and the movement characteristics theoretically predicted by the corresponding motor planning model. Nevertheless, a W_{NCF} value of just 1/4 still achieves a reasonable match with the theoretical result, indicating that even with MCFs the minimum search algorithm is working effectively.

4 Discussion

In the following, simulator performances in predicting WBP executions will be discussed and compared to analogous works previously proposed in literature. Moreover, some interesting neurophysiological implications of the new possibilities given by the simulator characteristics will be considered.

Reported results clearly show a remarkable accuracy of the proposed simulation technique. In fact, although it uses a biomechanical model with 5 DoFs, entailing a minimum search in a 70 (5 DoFs · 14 Coefficients of *B*-splines) dimension hyperspace, the simulator achieves consistent full minimizations, compatible with task fulfilment. Evidence of the simulator's reliability are the complete stabilization of CM and CP achieved when respective variances (σ^2_{CM} and σ^2_{CP}) are used as cost figures. In particular, the result related to σ^2_{CP}, which includes nonlinear components related to kinetics, clearly demonstrates that not only the simulator can efficiently handle the high

Table 2 The discrepancies between the theoretical results and the movements

W_{nCF1}–W_{nCF1}	0-1	1/4-3/4	1/2-1/2	3/4-1/4	1-0
RMSE Jerk (mm)	81.10	31.50	20.80	20.30	9.50
RMSE σ^2_{CP} (mm)	0.03	0.13	2.80	3.14	47.30

The theoretical results predicted by minimum endpoint jerk (Jerk) and minimum center of pressure displacement (σ^2_{CP}) models and the movements predicted by the simulator for 5 different combinations of the weights W_{nCFi} are reported here. The discrepancy are evaluated as root mean squared errors (RMSE)

Journal : Large 11517 Dispatch : 31-8-2007 Pages : 12
Article No. : 252 LE TYPESET
MS Code : 252 CP DISK

nonlinearities of the human motor system, but can exploit them to carry out the movement optimization.

Another useful characteristic of the proposed simulation technique is the possibility of imposing nonlinear constraints on the optimization problem. Indeed, this feature allows a simple, but effective, representation of human body anatomo-physiological characteristics. For instance, in addition to what has been done for many of the models proposed in literature [12, 22, 25, 30, 44, 51], the simulator takes into account the maximal torque that different muscular groups can exert at each joint angular position and velocity. Moreover, having been already highlighted the importance of using mathematical models that account for muscle dynamics [15], motor command-contraction dynamics is also implemented in the simulation method proposed here. The representation of the motor system intrinsic constraints seems especially important because it allows a more effective induction of the causes of the human motor behavior. Indeed, it gives the possibility to understand whether observed movement features are direct consequences of motor system characteristics, or whether they result from a specific strategy. For instance, it was demonstrated that human movement smoothness is strongly related to the nervous and muscular system features and not to an explicit CNS goal [17]. In the proposed simulator this specific consideration seems to be well represented by the imposed limits on the muscular inputs. Indeed, all simulator solutions, even when they aimed at optimizing critical movement aspects that do not explicitly include gracefulness (e.g., CM or CP stabilization), were never characterized by an unnatural jerkiness.

A further important aspect differentiating the proposed simulator from most similar works in the literature [17, 22, 25, 30, 32, 44, 51] is the validation of the biomechanical model representing human body segments and of the inverse/forward dynamic method (FDM). This procedure appears to be crucial, because inaccuracy in the estimation of joint torques would greatly affect the predictions obtained by implementing any motor planning model-based on movement kinetics [17, 25, 30, 48, 51] or energy [1, 42]. A further remark must be given on this topic. Although experimental evidences show that gravity determines relevant differences between upward and downward arm movements [34], most of the motor planning model used in literature, even those focusing on movement kinetics or energy [1, 30, 42, 51], do not consider the gravitational component of the joint torque or the variations in system potential energy. If this approximation was thought to be acceptable for arm movements, this is certainly not true for WBP. Therefore, the simulator's capacity to include gravitational effects seems indispensable to the study and modeling of motor-planning criteria underlying the execution of this category of movement.

Overall, the use of IDM to evaluate movement kinetics, instead of more classical FDMs, proves to be effective for the purposes of the present work. Indeed, the large number of DoFs of the multi-segment inverted pendulum representing the human body, as well as its intrinsic instability and nonlinearities, would make the use of the FDM inconvenient. Moreover, although it was already demonstrated that IDM and FDM agree if applied to the same model [5], the latest would require a huge computational power and the integration of feedback control techniques. Hence, it would restrain the simulator applicability because of the need for supercomputers with parallel processors [6, 32]. On the contrary, the proposed simulator can be run even on simple PCs: the results reported in this paper were obtained using a laptop with a Pentium 4 processor (2 GHz) and they took in average 24 ± 7 min.

The use of FDM would be necessary if the simulations were focused on the execution of movements in perturbed environments. In fact, in this case it would be necessary to include specific muscle models allowing modulations of the joint impedance through cocontraction and the stretch-reflex. Therefore, the implementation of motor control techniques such as the equilibrium point theory would be possible. However, since the aim of the present work is the prediction of the "desired trajectories" corresponding to optimization criteria in unperturbed conditions, the inclusion of these models does not seem of primary importance. Indeed, it was shown that joint impedance is preponderant in perturbed movements and it is minimized for unperturbed ones [8]. In the literature, this idea was even used to solve the third indeterminacy problem in simulation using FDM [3, 4, 32, 33] and, in general, to estimate muscle contributions to net joint torques [5, 11, 20, 33, 35, 50]. In particular, the third indeterminacy problem was solved by minimizing the global effort or the metabolic cost of movement. Since most of the planning criteria presented in the literature, for which the present simulator has been conceived, aim at solving just the two first indeterminacy problems [1, 12, 14, 17, 30, 42, 51], detailed models of each muscle, including uni- or bi-articular ones, and optimal force sharing criteria have not be integrated, though it would be theoretically possible.

In general, flexibility is a very important characteristics of the proposed simulation method. Although for simplicity and clarity reasons it is here applied to a bi-dimensional and symmetric movement, the simulator could also be employed for three-dimensional and asymmetric movements. In this case, the motion of the segments should be described also in terms of roll and yaw. Therefore, a line of the matrix **a** should be dedicated to the description of each of these angle trajectories. Moreover, in order to apply the IDM, the model segments should be characterized by their inertial moment in the frontal and horizontal planes. Also

Journal : Large 11517 Dispatch : 31-8-2007 Pages : 12
Article No. : 252 LE TYPESET
MS Code : 252 CP DISK

joint stiffness and viscosity in these two planes should be modelled. Accordingly, specific constraints on the joint range of motion and maximal torques should be included.

All results obtained for single motor planning criteria clearly show that the simulator integrates goal-oriented and postural components of the movement subordinating the equilibrium control to the endpoint trajectory generation (Jerk) or vice versa (σ^2_{CM}, σ^2_{CP}). For instance, wide and dangerous CP oscillations can be observed in simulations minimizing Jerk and large upper limb movement are predicted when the CM or CP stabilization is achieved. This could suggest that the criterion actually used by CNS to plan a whole body transitive movement should include both its goal-oriented and postural components. Furthermore, this hypothesis is in line with the idea proposed in literature that the true optimality criterion is likely to involve a mix of cost terms and that weights defining a multiattribute cost could be used as command signals by higher-level centers [47].

From this point of view, the demonstrated capability to combine different cost figures, using MCFs, seems to be particularly interesting, because it gives the possibility to test the validity of these theories also in the case of complex WBP task. In particular, results related to the simultaneous minimization of the hand trajectory jerkiness and the CP variance, although only illustrative and without any particular neurophysiological relevance, show the simulator's effectiveness in optimizing multiple cost functions. Indeed, the proposed combination technique succeeds in balancing the two MCF components and in producing a satisfactory gradual transition from one criterion to the other. However, it is important to notice that different characteristics of each of the motor planning criteria, such as specific nonlinearities of the cost function, could affect the results.

5 Conclusion

The proven efficacy and reliability of the proposed human movement simulator in identifying the "desired trajectories" corresponding to the optimization of various cost functions, strongly suggest that it could be effectively used to verify whether classical theories on motor planning could be extended to whole body movements involving several DoFs and requiring the coordination between task accomplishment and maintenance of balance. In addition, its capability of combining several optimality criteria seems especially interesting because it allows one to explore new motor control theories.

Moreover, the simulator's flexibility would allow its extension to further applications. For instance, it could be used to simulate various task. In particular, if the simulation technique was applied to a proper three-dimensional biomechanical model, the features of movements with relevant medio-lateral components could be predicted too. Also different force fields acting on the subject (e.g., hyper or micro-gravity) or subject motor deficits (e.g., weakening of specific muscle groups or reduction of joint mobility) could be easily implemented.

Acknowledgments The authors acknowledge J. McIntyre for his kind help.

References

1. Admiraal MA, Kusters MJMAM, Gielen SCAM (2004) Modeling kinematics and dynamics of human arm movements. Motor Control 8(3):312–338
2. Alexandrov A, Frolov A, Massion J (2001) Biomechanical analysis of movement strategies in human forward trunk bending. I. Modeling. Biol Cybern 84:425–434
3. Anderson FC, Pandy MG (1999) A dynamic optimization solution for vertical jumping in three dimensions. Comput Methods Biomech Biomed Eng 2(3):201–231
4. Anderson FC, Pandy MG (2001a) Dynamic optimization of human walking. J Biomech Eng 123(5):381–390
5. Anderson FC, Pandy MG (2001b) Static and dynamic optimization solutions for gait are practically equivalent. J Biomech 34(2):153–161
6. Anderson F, Ziegler J, Pandy M, Whalen R (1995) Application of high-performance computing to numerical simulation of human movement. J Biomech Eng 117:155–157
7. Atkeson C, Hollerbach J (1985) Kinematic features of unrestrained vertical arm movements. J Neurosci 5(9):2318–30
8. Burdet E, Osu R, Franklin DW, Milner TE, Kawato M (2001) The central nervous system stabilizes unstable dynamics by learning optimal impedance. Nature 414(6862):446–449
9. Coleman TF, Zhang Y (2003) Optimization Toolbox User's Guide. The MathWorks, Inc.
10. Commissaris D, Toussaint H, Hirschfeld H (2001) Anticipatory postural adjustments in a bimanual, whole-body lifting task seem not only aimed at minimising anterior–posterior centre of mass displacements. Gait Posture 14(1):44–55
11. Crowninshield DR, Brand RA (1981) A physiologically based criterion of muscle forze prediction in locomotion. J Biomech 14:793–801
12. Flash T, Hogan N (1985) The coordination of arm movements: an experimentally confirmed matematical model. J Neurosci 5:103–168
13. Ghafouri M, Archambault PS, Adamovich SV, Feldman AG (2002) Pointing movements may be produced in different frames of reference depending on the task demand. Brain Res 929(1):117–128
14. Gottlieb G, Song Q, Hong D, Almeida G, Corcos D (1996) Coordinating movement at two joints: a principle of linear covariance. J Neurophysiol 75(4):1760–4
15. Gribble P, Ostry D (1996) Origin of the power-law reaction between movement velocity and curvature—modeling the effects of muscle mechanics and limb dynamics. J Neurophysiol 76:2853–2860
16. Happee R (1994) Inverse dynamic optimization including muscular dynamics, a new simulation method applied to goal directed movements. J Biomech 27(7):953–960
17. Harris CM, Wolpert DM (1998) Signal-dependent noise determines motor planning. Nature 394(6695):780–784

Journal : Large 11517 | Dispatch : 31-8-2007 | Pages : 12
Article No. : 252 | LE | TYPESET
MS Code : 252 | CP | DISK

18. Hoy M, Zajac F, Gordon M (1990) A musculoskeletal model of the human lower extremity: the effect of muscle, tendon and moment arm on the moment-angle relationship of musculotendon actuators at the hip, knee and ankle. J Biomech 23(2):157–169
19. Kaminski TR, Simpkins S (2001) The effects of stance configuration and target distance on reaching. I. Movement preparation. Exp Brain Res 136(4):439–446
20. Kaufman KR, An KN, Litchy WJ, Chao EY (1991) Physiological prediction of muscle forces—II. Application to isokinetic exercise. Neuroscience 40(3):793–804
21. Kerlirzin Y, Pozzo T, Dietrich G, Vieilledent S (1999) Effects of kinematics constraints on hand trajectory during whole-body lifting tasks. Neurosci Lett 277(1):41–44
22. Koopman B, Grootenboer HJ, de Jongh HJ (1995) An inverse dynamics model for the analysis, reconstruction and prediction of bipedal walking. J Biomech 28:1369–1376
23. Kuo A (1998) A least-squares estimation approach to improving the precision of inverse dynamics computations. J Biomech Eng 120(1):148–59
23. Lashley K (1951) Cerebral mechanisms in behaviour, Jeffress (ed) Wiley, New York, chap The problem of serial order in behaviour
25. Lo J, Huang G, Metaxas D (2002) Human motion planning based on recursive dynamics and optimal control techniques. Multibody System Dynamics 8:433–458
26. Marshall R, Mazur S, Taylor N (1990) Three-dimensional surfaces for human muscle kinetics. Eur J Appl Physiol 61:263–270
27. Massion J (1992) Movement, posture and equilibrium: interaction and coordination. Progress Neurobiol 83:35–56
28. Massion J, Popov K, Fabre JC, Rage P, Gurfinkel V (1997) Is the erect posture in microgravity based on the control of trunk orientation or center of mass position? Exp Brain Res 114(2):384–389
29. Morasso P (1981) Spatial control of arm movement. Exp Brain Res 42:223–227
30. Nakano E, Imamizu H, Osu R, Uno Y, Gomi H, Yoshioka T, Kawato M (1999) Quantitative examinations of internal representations for arm trajectory planning: minimum commanded torque change model. J Neurophysiol 81(5):2140–2155
31. Otis J, Warren R, Backus S, Santner T, Mabrey J (1990) Torque production in the shoulder of the normal young adult male. The interaction of function, dominance, joint angle, and angular velocity. Am J Sports Med 18(2):119–123
32. Pandy M (2001) Computer modeling and simulation of human movement. Annu Rev Biomed Eng 3:245–73
33. Pandy M, Sim FZE, Levine W (1990) An optimal control model for maximum-height human jumping. J Biomech 23(12):1185–98
34. Papaxanthis C, Pozzo T, Stapley P (1998) Effects of movement direction upon kinematic characteristics of vertical arm pointing movements in man. Neurosci Lett 253(2):103–106
35. Pedotti A, Krishnan V, Stark L (1978) Optimization of muscle-force sequencing in human locomotion. Math Biosci 38:57–76
36. Pozzo T, McIntyre J, Cheron G, Papaxanthis C (1998) Hand trajectory formation during whole body reaching movements in man. Neurosci Lett 240(3):159–162
37. Pozzo T, Stapley PJ, Papaxanthis C (2002) Coordination between equilibrium and hand trajectories during whole body pointing movements. Exp Brain Res 144(3):343–350
38. Ramos C, Stark L (1990) Postural maintenance during fast forward bending: a model for simulation experiment determines the 'reduced trajectory'. Exp Brain Res 82:651–657
39. Riener R, Fuhr T (1998) Patient-driven control of fes-supported standing up: a simulation study. IEEE Trans Rehabil Eng 6(2):113–124
40. Riener R, Edrich T (1999) Identification of passive elastic joint moments in the lower extremities. J Biomech 32(5):539–544
41. Soechting JF, Lacquaniti F (1981) Invariant characteristics of a pointing movement in man. J Neurosci 1(7):710–720
42. Soechting JF, Buneo CA, Herrmann U, Flanders M (1995) Moving effortlessly in three dimensions: does donders' law apply to arm movement? J Neurosci 15(9):6271–6280
43. Stapley P, Pozzo T, Grishin A (1998) The role of anticipatory postural adjustments during whole body forward reaching movements. Neuroreport 9(3):395–401
44. Stapley P, Pozzo T, Grishin A, Papaxanthis C (2000) Investigating centre of mass stabilisation as the goal of posture and movement coordination during human whole body reaching. Biol Cybern 82(2):161–172
45. Thomas JS, Corcos DM, Hasan Z (2003) Effect of movement speed on limb segment motions for reaching from a standing position. Exp Brain Res 148(3):377–387
46. Thomas JS, Corcos DM, Hasan Z (2005) Kinematic and kinetic constraints on arm, trunk, and leg segments in target-reaching movements. J Neurophysiol 93(1):352–364
47. Todorov E (2004) Optimality principles in sensorimotor control. Nat Neurosci 7(9):907–915
48. Todorov E, Jordan MI (2002) Optimal feedback control as a theory of motor coordination. Nat Neurosci 5(11):1226–1235
49. Toussaint H, Michies Y, Faber M, Commissaris D, van Dieën J (1998) Scaling anticipatory postural adjustments dependent on confidence of load estimation in a bi-manual whole-body lifting task. Exp Brain Res 120(1):85–94
50. Tsirakos D, Baltzopoulos V, Bartlett R (1997) Inverse optimization: functional and physiological considerations related to the force-sharing problem. Crit Rev Biomed Eng 25(4-5):371–407
51. Uno Y, Kawato M, Suzuki R (1989) Formation and control of optimal trajectory in human multijoint arm movement. Minimum torque-change model. Biol Cybern 61(2):89–101
52. Unser M, Aldroubi A, Eden M (1993) B-spline signal processing: part I—theory. IEEE Trans Signal Process 41(2):821–833
53. Zatsiorsky V, Seluyanov V (1983) The mass and inertia characteristics of the main segments of the human body. Biomechanics VIII-B. In: Matsui H, Kobayashi K (eds) Kinetics of human motion, Human Kinetic Publishers, pp 1151–1159
54. Zhang LQ, Rymer WZ (1997) Simultaneous and nonlinear identification of mechanical and reflex properties of human elbow joint muscles. IEEE Trans Biomed Eng 44(12):1192–1209
55. Zhang LQ, Nuber G, Butler J, Bowen M, Rymer WZ (1998) In vivo human knee joint dynamic properties as functions of muscle contraction and joint position. J Biomech 31(1):71–76

Journal : Large 11517 | Dispatch : 31-8-2007 | Pages : 12
Article No. : 252 | ☐ LE | ☐ TYPESET
MS Code : 252 | ☑ CP | ☑ DISK